Interatomic potentials and the simulation of fracture: C15 $NbCr_2$

Frohmut Rösch and Hans-Rainer Trebin
Institut für Theoretische und Angewandte Physik, Universität Stuttgart,
Pfaffenwaldring 57, 70550 Stuttgart, Germany

Peter Gumbsch
Institut für Zuverlässigkeit von Bauteilen und Systemen,
Universität Karlsruhe, Kaiserstr. 12, 76131 Karlsruhe, Germany
Fraunhofer Institut für Werkstoffmechanik, Wöhlerstr. 11, 79108 Freiburg, Germany

preprint

Abstract

The discrete nature of solids and the interatomic interactions strongly influence crack propagation. Lattice trapping results in stable cracks above and below the critical Griffith load. Local atomic arrangements near the crack front define fracture behaviour. The analysis of these processes on an atomic scale helps to understand principle mechanisms and their consequences, which also have to be incorporated in more coarse-grained descriptions to get reliable results. Large-scale molecular dynamics simulations of fracture on the atomic level can supply information not accessible to experiment. But to simulate a specific material reasonable effective interatomic potentials are needed. In this paper we report on the fitting and validation of potentials specifically generated for the fracture of C15 $NbCr_2$. Results are compared to those derived with potentials for the elements from the literature. The comparison indicates that interactions fitted to elemental metals are not sufficient to determine alloy properties.

1 Introduction

Intermetallic compounds frequently combine interesting properties like high melting point, high temperature strength, and low density. However, possible applications are then often limited by extreme brittleness at low or ambient temperature. As fracture is ultimately determined by the breaking of bonds, an understanding of the fundamental mechanisms on this atomic level is required. For such studies molecular dynamics simulation is a promising method. Although with this technique insight has been gained in fracture of simple structures and model systems, the situation in complex metallic alloys is less clear. In some detail only model quasicrystals and Laves phases have been investigated with model potentials [1–3].

One reason for this situation is the lack of suitable interatomic potentials. Here, one is usually directed to so-called realistic effective potentials which are adjusted to experimental or ab-initio data. Such pair or embedded atom method (EAM) type potentials [4] are nearly always expressed by analytical functions that were fitted to at most a dozen material properties known from experiment or ab-initio calculations. However, these potentials may then

only be valid for defect-free bulk materials and for their equilibrium properties. In simulations of extreme conditions – like fracture of materials – such "realistic" potentials may lead to questionable results. Another problem is that they were often derived for elemental metals and then extended to intermetallic compounds.

One way out of this dilemma is the use of model potentials. In fracture simulations simple model potentials (e.g. Lennard-Jones) with a deep first minimum and a repulsive core part in many cases outperform more sophisticated potentials. Such a choice is appropriate if qualitative aspects of the structure are the centre of interest and the depths and minima of the potentials have been adjusted to keep the structure stable. Nevertheless, clear disadvantages are the neglect of many-body interactions and the impossibility to derive quantitative results for a specific material.

Another way to simulate fracture of complex metallic alloys is to use potentials directly force-matched [5] to ab-initio data from the intermetallic compound. We will report on this issue for the Laves phase C15 $NbCr_2$ and compare results to simulations using EAM potentials for the elemental metals from the literature.

2 EAM potentials and the force-matching method

EAM type potentials [4] describe interactions with a pair term, which depends only on the distance between particles, and an additional embedding term. The latter one leads to forces acting on the host particle by embedding it in the sea of "electrons" provided by the neighbouring atoms, which is described by the so-called transfer functions. Therefore, the embedding function includes many-body interactions without explicit angular dependences. In such a physical interpretation of the semi-empiric EAM formulation it is often stated that the pair term represents the core repulsion. However, because of gauge degrees of freedom, these "core" and "electronic" contributions are not uniquely defined. One can motivate the mathematical form of EAM potentials from quantum-mechanical calculations. Dependent on the assumptions and the derivation in the literature different analytical expressions for the functions are used, whereas the potential energy U is always formulated as follows:

$$U = \sum_{i,j<i}^{N} \phi_{k_i k_j}(r_{ij}) + \sum_{i}^{N} F_{k_i}(\rho_i^h) \left(+ \sum_{i}^{N} M_{k_i}(q_i^h) \right) \tag{1}$$

$$\text{where} \qquad \rho_i^h = \sum_{j \neq i}^{N} P_{k_j}^{at}(r_{ij}) \tag{2}$$

$$\text{and} \qquad q_i^h = \sum_{j \neq i}^{N} \left(P_{k_j}^{at}(r_{ij}) \right)^2 \tag{3}$$

Here $\phi_{k_i k_j}$ is the pair potential, which depends on the atomic species k_i, k_j of the atoms i and j and the distance r_{ij} between them. F_{k_i} is the embedding function depending on the host density ρ_i^h of atom i, which is a sum over the transfer functions $P_{k_j}^{at}$ of the neighbouring atoms j. The term in brackets is an extension of the original EAM formulation (see Sec. 4), which includes additional embedding functions M_{k_i}, that depend on the sum q_i^h of the squared transfer functions.

Within the force-matching method we first determine forces, total energies, and the components of the pressure tensor for diverse representative configurations by ab-initio calcula-

tions. This data is then used to match potentials minimising the deviations from the ab-initio reference values in the same configurations. The choice of reference samples allows for potentials for special purposes and is crucial for their reliability. For the ab-initio part, we perform density-functional theory (DFT) calculations within the generalised gradient approximation (GGA) for the exchange-correlation energy using the Vienna Ab-initio Simulation Package VASP [6–8]. For Nb and Cr we apply projector augmented wave (PAW) potentials, which treat the semi-core p states as valence. The maximal energy cutoff is increased by 30%. Our samples consist of 24 to 144 atoms. The **k**-mesh is automatically generated using the Monkhorst-Pack scheme with up to $5 \times 5 \times 5$ points. Under the 50 configurations used there are compressed, elongated, and sheared samples; vacancies are included and atoms are exchanged. Especially, we also carried out calculations for free surfaces. To overcome the number of limited environments in ordered structures, samples at higher temperatures are used to obtain sufficient information on forces at various interaction distances. In addition, to get some sort of "cohesion" energy, the energies of single atoms in a triclinic box are calculated. This data is used as input for the program *potfit* which is developed in our group by P. Brommer and F. Gähler [9]. It generates EAM potentials with cubic splines using conjugate gradient and simulated annealing techniques within a least-squares method. The forces on each atom, total energies, and pressures are calculated for the generated potentials and compared to the reference values in the same configurations. The number of sampling points used for the pair and transfer functions is typically about 15, the corresponding value for the embedding functions is about 10. To assure that the obtained potentials are defined even for extreme cases they are manually extended: The pair potential for short distances with a term proportional to r_{ij}^{-12}, the transfer functions for short distances and the embedding functions for high densities with terms linear in r_{ij} and ρ_i^h.

3 The Friauf-Laves phases

The Friauf-Laves phases are often only named Laves phases, though they were discovered by Friauf [10, 11] but extensively studied by Laves [12, 13]. They are formed by elements whose atomic diameters are approximately in the ratio of 1.2:1. Hence they often are termed size components. There are three main structural variants corresponding to $MgZn_2$ (C14), $MgCu_2$ (C15), and $MgNi_2$ (C36). They can be described by different stackings of layers (see e.g. [14, 15]) similarly to the relationship between face-centred cubic and hexagonal close packed structures. In the Laves phases BS_2 two kinds of layers are present formed by a Kagomé and a triangular net. The stacking sequences can be described as follows:

$$\text{C14, hexagonal:} \quad \alpha\, A\, \alpha \quad c \quad \beta\, B\, \beta \quad c \quad ... \tag{4}$$

$$\text{C15, cubic:} \quad \alpha\, A\, \alpha \quad c \quad \beta\, B\, \beta \quad a \quad \gamma\, C\, \gamma \quad b \quad ... \tag{5}$$

$$\text{C36, dihexagonal:} \quad \alpha\, A\, \alpha \quad c \quad \beta\, B\, \beta \quad c \quad \alpha\, A\, \alpha \quad b \quad \gamma\, C\, \gamma \quad b \quad ... \tag{6}$$

Here upper case letters represent Kagomé and lower case letters triangular nets. Layers of big B atoms are represented by greek and those of small S atoms by latin letters. The letter itself indicates the in-plane position of the atoms in the layer. In the C15 structure the B atoms form a diamond lattice, whereas the S atoms build a tetrahedral network. The Laves phases can also be formed by prolate rhombohedra [16, 17] but not in a uniquely defined way. Because of the already quite complex structure new deformation modes like synchro-shearing (see e.g. [18]) might emerge.

The choice of a specific material was guided by a possible relevance for technical applications and the compatibility with EAM potentials. Anomalous shear moduli and strong electron-phonon coupling e.g. exclude C15 HfV_2 and ZrV_2 [19]. Literature search lead to the choice of C15 $NbCr_2$. Though the interatomic interactions are difficult to describe for the body centred cubic metals Nb and Cr [20–23], these elements seem favourable for the simulation of the C15 Laves phase because of the rather simple electronic [24, 25] and spatially close-packed structure of $NbCr_2$. Here, one has to emphasize again that we match potentials for the Laves phase and not for the elemental metals. Thus we do not claim that the generated potentials – especially those for the Cr interactions – are transferable to them.

4 Validation of the potentials

The potentials for $NbCr_2$ – that we force-matched to ab-initio data as described in Sec. 2 – are shown in Fig. 1. In addition to these "fm-EAM" potentials, analytical EAM potentials for the elemental metals taken from the literature (see [26, 27]) are shown in Fig. 2. To account for the difference between the actual total energy of a system of atoms and that calculated from the original EAM Yifang and co-workers [26, 27] included additional embedding functions M_{k_i} (see Eqs. (1) and (3)). This extended version of the EAM potentials will in the following be termed "e-EAM". With the fm-EAM and e-EAM potentials we carried out molecular dynamics simulations with the program code IMD [28, 29].

The lattice constant of $NbCr_2$ is derived by scaling the infinitely repeated unit cell, such that the pressure vanishes and the potential energy reaches its minimum. The fm-EAM potentials result in a lattice constant a_{lattice} of 6.94 Å, the e-EAM potentials give 6.79 Å. The elastic constants were deduced from three independent deformations as described in [30]. The obtained values are $C_{11} = 300$ GPa, $C_{12} = 181$ GPa, and $C_{44} = 55$ GPa for the fm-EAM potentials, whereas they are $C_{11} = 558$ GPa, $C_{12} = 259$ GPa, and $C_{44} = 102$ GPa for the e-EAM potentials. Thus, the values obtained for the e-EAM potentials are noticeably larger. These results are also shown in Tab. 1 together with ab-initio and experimental data. The three ab-initio results presented there (columns VASP, Hong et al. [30], and Mayer et al. [31]) are in good agreement. Small deviations are due to different methods and approximations in the ab-initio calculations and determinations of the elastic constants. Experimental data is also reproduced correctly. In comparison it is directly evident from Tab. 1 that the values obtained for the fm-EAM potentials generated by us correspond to ab-initio and experimental data very well, whereas the e-EAM potentials give a lower lattice constant and too high values for the elastic constants. For the simulation of fracture also elastic properties at large strains may play a significant role. To investigate this behaviour we scale the coordinates of the atoms by $1 + \alpha$, keep them fixed, and then calculate the pressure. The obtained stress-strain relationship is rather artificial as the atoms would move and relax in a molecular dynamics simulation. Nevertheless, it has been shown by Abraham [34] that e.g. the instability onset of brittle fracture is related to the corresponding secant modulus at the stability limit. For the fm-EAM potentials the maximum stress is at about 38 GPa at 18% strain, which is in agreement with ab-initio calculations (see Fig. 3, left). The values for the e-EAM potential are higher but seem nevertheless to be quite reasonable. For small strains it is again obvious, that the e-EAM potentials overestimate the elastic constants. A stress-strain relationship for uniaxial strain is shown in Fig. 3, right. There the coordinates are only scaled in [010] direction by $1 + \beta$. Again, the maximum for the fm-EAM potentials is closer to the ab-initio value than

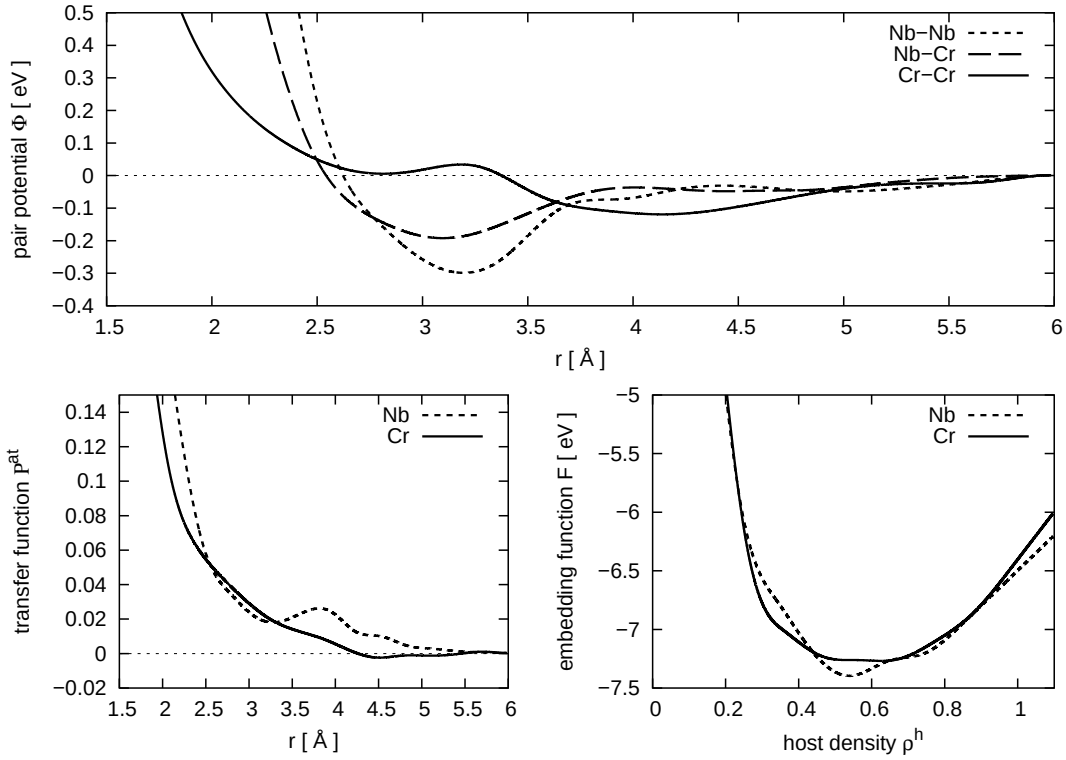

Figure 1: Force-matched EAM (fm-EAM) potentials for $NbCr_2$.

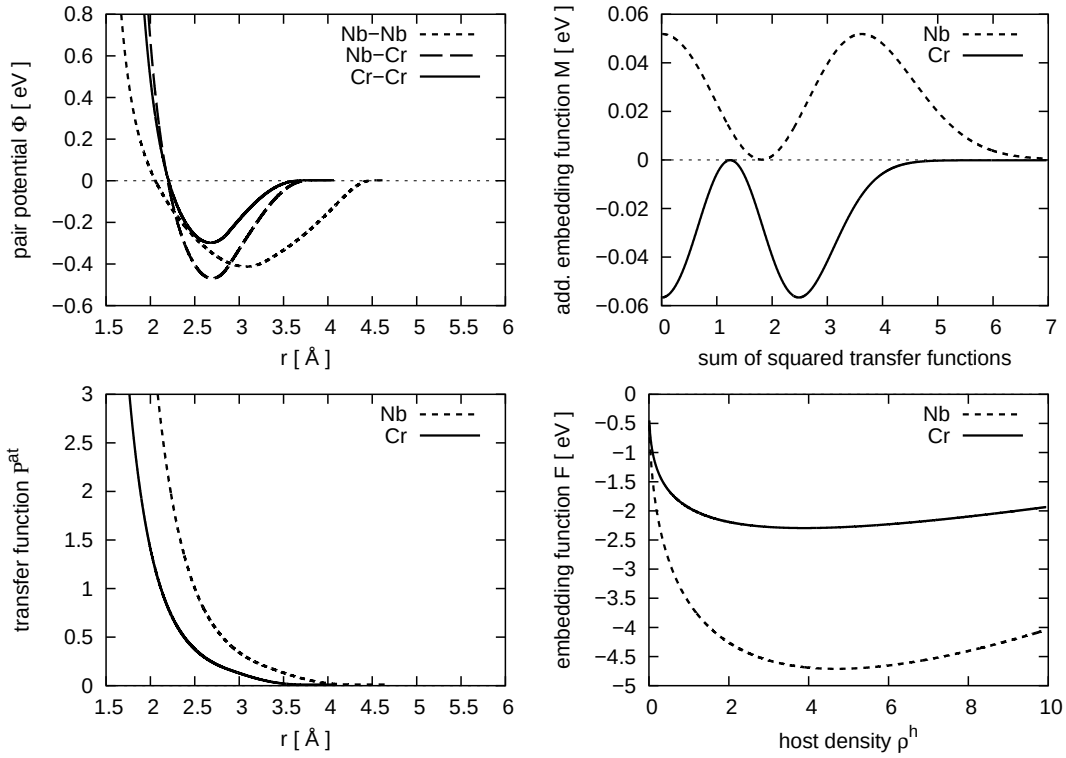

Figure 2: Analytical EAM (e-EAM) potentials for Nb-Nb, Cr-Cr, and Nb-Cr interactions [26, 27].

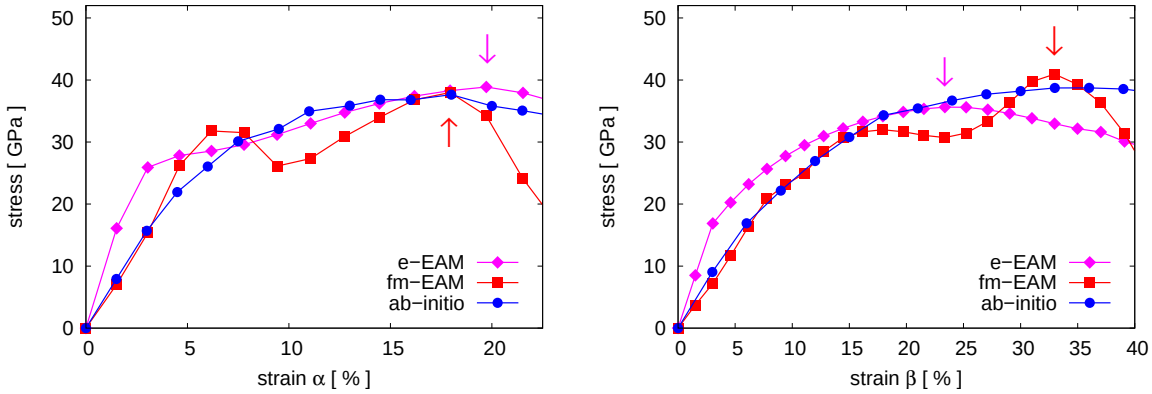

Figure 3: (Colour online) In the stress-strain diagrams the arrows mark the global stress maxima. For details, see text.

the one for the e-EAM potentials. Additionally, up to half of the corresponding strain the fm-EAM stresses coincide with the ab-initio values. However, it is also directly apparent from the figures that the e-EAM potentials result in a smoother behaviour than the fm-EAM potentials in the intermediate range of strains. This is due to the artifical calculation of the stress-strain relationship in which the atoms are kept fixed, due to the analytical expressions used for the e-EAM potentials, and due to their shorter interaction range. Increasing this range can help e.g. to distinguish systems with different stackings of layers (see Sec. 3). Potentials with additional features in their long-range part also can help to stabilise structures. For example, the simple pairwise Dzugutov potential [35] is able to favour bcc [36] over close-packed structures like fcc. This is achieved by an additional maximum in the potentials at a larger distance. An advantage of the force-matching method (see Sec. 2) is that one is able to define a reasonable interaction range. Potentials that are essentially zero after a certain distance may be truncated. The long-range part of the potentials, however, will also alter e.g. stress-strain curves. Thus, that these are a bit wavy for the fm-EAM potentials may be seen as a direct consequence of trying to describe accurately both equilibrium properties as well as the behaviour at e.g. large strains or high temperatures.

As we want to perform fracture simulations at low temperature, the melting temperature has not necessarily to be resembled well. Nevertheless, as the region near the crack tip can get very hot, the melting temperature T_{melt} at vanishing pressure should not be too low. Determining T_{melt} with atomistic simulations may lead to some difficulties (see e.g. [37, 38]). However, an upper limit for it can be determined by NPT-simulations by gradually and slowly increasing the temperature of a bulk sample. When the sample is melting, a distinct jump in the volume and in the mean square displacements can be observed. But, as there are no free surfaces present, the nucleation in the melting process is hindered (see e.g. [39]). Even for monoatomic bulk Al it was reported [38] that the solid phase could be heated to temperatures 500 K above the melting temperature. Furthermore, $NbCr_2$ transforms from a C15 to a C14 structure before melting (see e.g. [32]). It is questionable if EAM potentials are capable of describing this behaviour satisfactorily. Anyway, the limited time scale of molecular dynamics simulations may make it difficult to be observed. The evaluated temperature may thus only yield an upper bound for the melting temperature. With this in mind the obtained values (see Tab. 1) may be reasonable for both e-EAM and fm-EAM potentials. However,

Table 1: Results obtained for fm-EAM and e-EAM potentials, ab-initio and experimental data for bulk C15 $NbCr_2$. B is the bulk modulus. V and R denote Voigt and Reuss averages of Young's modulus E and the shear modulus G; Hill values are given where only one number appears.

	fm-EAM	e-EAM	VASP	Hong et al. [30]	Mayer et al. [31]	exp. [32, 33]
a_{lattice} [Å]	6.94	6.79	6.97	6.82	6.82 - 6.92	6.99
C_{11} [GPa]	300	558	309	316	316 - 322	–
C_{12} [GPa]	181	259	198	216	185 - 216	–
C_{44} [GPa]	55	102	69	71	69 - 83	–
B [GPa]	221	359	235	249	229	229.4
$E_{\text{V/R}}$ [GPa]	157/157	326/316	175/173	173/168	205	214.1
$G_{\text{V/R}}$ [GPa]	57/57	121/117	64/63	62/61	76	79.6
$k_{\text{B}}T_{\text{melt}}$ [eV]	< 0.24	< 0.17	–	–	–	0.176
	0.17	0.10				

the value for the e-EAM potential is already too low and that for the fm-EAM potentials seems too high. The melting temperature can also be determined with the help of two-phase systems. There a solid-liquid interface exists, so that some of the above mentioned problems can be circumvented. To determine the melting temperature of such a system, we prepare a periodically repeated cubic box. A central ball consists of the solid C15 Laves phase and the rest is filled with the molten sample. Then various NPT-simulations at constant temperatures near the melting temperature and at zero pressure are performed. If the central region totally melts the temperature is already above the melting temperature. The observation and simulation time is limited to a maximum of 30 ns. The samples consist of about 24 000 atoms. The thus obtained values for the melting temperature are also given in Tab. 1. With $k_{\text{B}}T_{\text{melt}} = 0.17$ eV the experimental data is resembled very well by the fm-EAM potentials, whereas the value for the e-EAM potentials is too low.

Apart from the reliable representation of bulk properties, free surfaces have to be stabilised when material is fractured. Especially, no atoms should evaporate. This is not guaranteed for effective pair potentials which lack a deep first minimum. Close-packed (111) surfaces are stabilised by both the fm-EAM and the e-EAM potentials. However, the atoms near the surfaces relax quite differently. This is shown in Fig. 4: Grey (online: red) and black (online: blue) circles represent Cr and Nb atoms in the initial sample, the bright (online: yellow) spots indicate the relaxed positions. The fm-EAM potentials lead to a relaxation of the two top layers of atoms towards the bulk. This behaviour is confirmed by ab-initio results (compare left and bottom configurations in Fig. 4). Using the e-EAM potentials the first layer of Cr atoms moves away from the bulk, the first layer of Nb atoms moves inwards. When carefully looked-at changes in the remaining layers can also be observed in Fig. 4.

To test whether this difference in relaxation also manifests itself in fracture behaviour, we perform comparative simulations. A strip geometry is used to model crack propagation with constant energy release rate. The length of the strips l is set to about 0.1 µm. The dimensions of the samples are approximately $l \times \frac{l}{3} \times \frac{l}{6}$ and contain nearly 5 million particles. Periodic boundary conditions are applied in the direction parallel to the crack front. For the other directions, atoms in the outermost boundary layers of width 6 Å are held fixed. An atomically sharp seed crack is inserted from one side to about $l/4$. The system is uniaxially

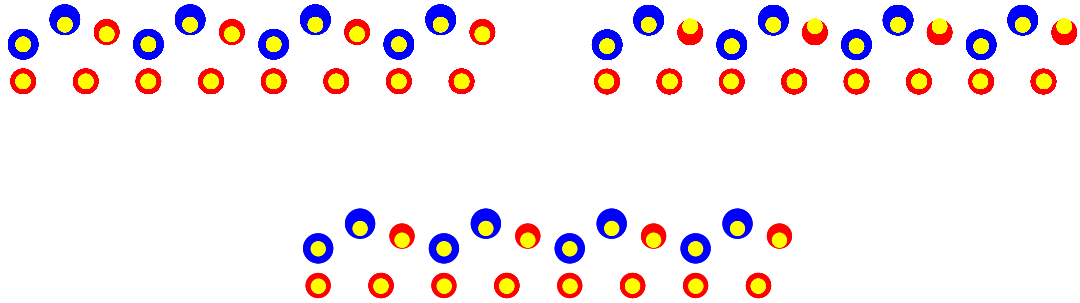

Figure 4: (Colour online) Relaxation of a (111) surface using fm-EAM potentials (left), e-EAM potentials (right), and ab-initio molecular dynamics (bottom).

strained perpendicular to the crack plane up to the Griffith load (see below) and relaxed. The mode I crack then is further loaded by scaling the displacement field of the stable crack at low temperature. Details of the molecular dynamics simulation technique can be found in [2].

The total surface energy γ_{tot} needed to generate two flat, unrelaxed (111) surfaces is minimal for a cut between a Kagomé and a triangular net. Thus, the initial seed crack is inserted there. The corresponding $\gamma_{\mathrm{tot}}^{\mathrm{min}}$ is $4.4\,\mathrm{J/m^2}$ for the e-EAM potentials and $5.6\,\mathrm{J/m^2}$ for the fm-EAM potentials. Preliminary ab-initio values calculated by A. Al-Zu'bi et al. [40] indicate that $\gamma_{\mathrm{tot}}^{\mathrm{min}}$ might even be about 30% higher than the fm-EAM result. As surface energies are hard to fit even with EAM potentials, the fm-EAM value seems acceptable, while the e-EAM result is even lower. Following Griffith [41], the energy release rate required for fracture is γ_{tot}. However, the discreteness of the lattice manifests itself in the so-called lattice-trapping effect [42]. It causes cracks to remain stable in a region around the critical Griffith load K_{G}. Thus, to initiate crack propagation, a stress intensity factor $K > K_{\mathrm{G}}$ is required. Lattice trapping also can vary for different crack propagation directions within a given cleavage plane. Experimental results give fracture toughness values for $NbCr_2$ alloys between 1 and 2 $\mathrm{MPa}\sqrt{\mathrm{m}}$ [43, 44].

The seed crack for the fm-EAM potentials propagates in $[2\bar{1}\bar{1}]$ direction for $K \geq 1.2\,K_{\mathrm{G}}$. Hence the energy release rate needed for crack propagation is about 1.4 times the Griffith value. The surplus of energy indicates that fracture surfaces with $\gamma_{\mathrm{tot}} > \gamma_{\mathrm{tot}}^{\mathrm{min}}$ can be realised. Atoms near the crack tip are selected by their coordination number and then visualised in Fig. 5. The fm-EAM potentials give brittle cleavage fracture with no indication of any dislocation activity (see inset). The observed change to a parallel plane does not alter γ_{tot}, as this corresponds to cuts between $\alpha\,A$ or $A\,\alpha$ in the C15 stacking sequence (see Sec. 3). The surfaces of the fractured sample are geometrically scanned with a Nb atom. A small square section with an edge length of about 5 nm is shown in Fig. 5. The Kagomé net (with a few defects) is clearly visible.

At first glance the seed crack for the e-EAM potentials seems to emit a dislocation for $K = 1.1\,K_{\mathrm{G}}$ (see Fig. 5). Crack propagation resulting in rough fracture surfaces only is observed for very high loads (e.g. $K = 1.8\,K_{\mathrm{G}}$). Thus, the brittle behaviour of the fm-EAM material is opposed to the more ductile manner of the e-EAM sample. However, it is known from experiment that $NbCr_2$ is brittle up to about 2/3 of the melting temperature and fails

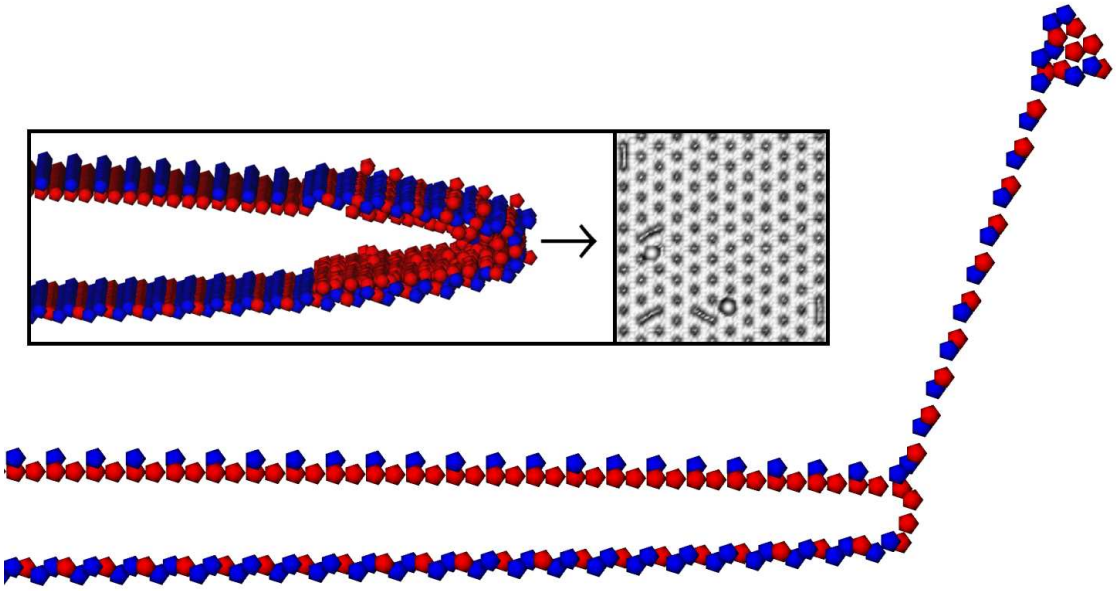

Figure 5: (Colour online) Atomic configurations near a crack tip using e-EAM and fm-EAM (inset) interactions. Surface of the seed crack: (111). The arrow indicates crack propagation in $[2\bar{1}\bar{1}]$ direction.

by macroscopic fracture (see e.g. [45]). Hence the e-EAM potentials here yield questionable results. This indicates that the use of effective, analytical EAM potentials for elemental metals can even result in qualitatively wrong behaviour when used for simulations of intermetallic compounds. For a closer inspection of the faulted sample near the e-EAM crack, atomic configurations close to the defect are shown in Fig. 6 (right). The initial positions of the atoms are also depicted (Fig. 6, left). The horizontal lines indicate atomic $(\bar{1}11)$ layers, the vertical lines help to determine the layer type. The stacking sequences are given below the pictures. In the initial sample (left) the stacking sequence (from bottom to top beginning with the first horizontal line) resembles the C15 structure of $NbCr_2$ (see Eq. (5)). In the faulted sample (Fig. 6, right) the upper half is shifted by $\mathbf{b} = a_{\text{lattice}}/6 \cdot [211]$ relatively to the lower half, which corresponds to a Shockley partial. However, the failure mechanism cannot be described by a simple dislocation and is also not compatible with synchro-shearing. As can be seen in the right part of Fig. 6 and in the stacking sequence given below, layers in the middle of the configuration are exchanged. This is the reason why only two layers of atoms mark the fault in Fig. 5. The coordination number of Nb and Cr atoms is different, therefore, by exchanging the layers, they lose their usual coordination and then are displayed. For the other atoms the coordination number stays the same. This exchange of layers leads to a stacking sequence $(c\alpha)\beta$ that is not present in any Laves phase (compare to Eqs. (4),(5), and (6)) and can be interpreted as a consequence of the relative movements of the atomic layers at a surface as shown in Fig. 4. Thus, this local phase transformation can be regarded as an artefact of the e-EAM potentials used.

The results mentioned above indicate that the fm-EAM potentials force-matched to ab-initio data for $NbCr_2$ are much more reliable than the analytical e-EAM potentials for Nb and

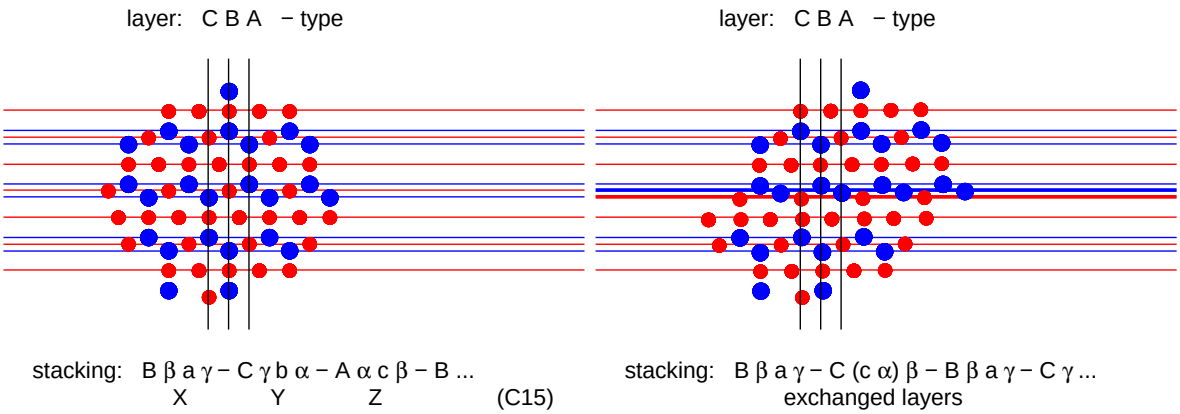

Figure 6: (Colour online) Stacking sequence before and after (see Fig. 5) the loading of a crack using e-EAM potentials.

Cr when properties of the intermetallic compound are of interest. The latter may then even result in qualitatively wrong results. The fm-EAM potentials also resemble well ab-initio and experimental data.

5 Conclusions

In conclusion, we have shown that the force-matching method is a promising – though time-consuming – method to derive EAM potentials for intermetallic compounds. When simulating complex metallic alloys a careful choice of potentials is necessary. Interactions fitted to elemental metals can lead to wrong or at least questionable results. Therefore the use of so-called "realistic" potentials for the elements does not guarantee that the results for compounds are reliable. This paper proves that in the case of C15 $NbCr_2$ available potentials for the elemental metals are outperformed by our force-matched potentials. These are thus currently used to perform a systematic study on crack propagation in this compound.

Acknowledgements

F. R. wants to thank Dr. Franz Gähler and Peter Brommer for the program *potfit* and appreciates helpful discussions with Prof. Dr. Christian Elsässer and Prof. Dr. Farid F. Abraham. Financial support from the Deutsche Forschungsgemeinschaft under contract number TR 154/20-1 is gratefully acknowledged.

References

[1] F. Rösch, Ch. Rudhart, P. Gumbsch, and H.-R. Trebin, Mat. Res. Soc. Symp. Proc. **805**, LL9.3 (2004).

[2] F. Rösch, Ch. Rudhart, J. Roth, H.-R. Trebin, and P. Gumbsch, Phys. Rev. B **72**, 014128 (2005).

[3] F. Rösch, H.-R. Trebin, and P. Gumbsch, Phil. Mag. **86** (6-8), 1015–1020 (2006).

[4] M. S. Daw and M. I. Baskes, Phys. Rev. Lett. **50** (17), 1285–1288 (1983).

[5] F. Ercolessi and J. B. Adams, Europhys. Lett. **26** (8), 583–588 (1994).

[6] G. Kresse and J. Furthmüller, Comp. Mat. Sci. **6** (1), 15–50 (1996).

[7] G. Kresse and D. Joubert, Phys. Rev. B **59** (3), 1758–1775 (1999).

[8] VASP – the Vienna Ab-initio Simulation Package: http://cms.mpi.univie.ac.at/vasp/

[9] P. Brommer and F. Gähler, Phil. Mag. **86** (6-8), 753–758 (2006).

[10] J. B. Friauf, Phys. Rev. **29** (1), 34–40 (1927).

[11] J. B. Friauf, J. Am. Chem. Soc. **49** (12), 3107–3114 (1927).

[12] F. Laves and H. Witte, Metallwirtsch. **14** (33), 645–649 (1935).

[13] F. Laves and H. Witte, Metallwirtsch. **15** (36), 840–842 (1936).

[14] P. M. Hazzledine and P. Pirouz, Scripta Metall. et Mater. **28** (10), 1277–1282 (1993). Be aware of some typing errors in the text.

[15] J. D. Livingston, Phys. Stat. Sol. A **131**, 415–423 (1992).

[16] C. L. Henley and V. Elser, Phil. Mag. B **53** (3), L59–L66 (1986).

[17] Q. B. Yang and K. H. Kuo, Acta Cryst. A **43** (6), 787–795 (1987).

[18] M. F. Chisholm, S. Kumar, and P. Hazzledine, Science **307**, 701–703 (2005).

[19] F. Chu, T. E. Mitchell, S. P. Chen, M. Sob, R. Siegl, and D. P. Pope, Mat. Res. Soc. Symp. Proc. **364**, 1389–1394 (1995).

[20] M. I. Baskes, J. S. Nelson, and A. F. Wright, Phys. Rev. B **40** (9), 6085–6100 (1989).

[21] J. B. Adams and S. M. Foiles, Phys. Rev. B **41** (6), 3316–3328 (1990).

[22] H. L. Alberts, J. Phys.: Cond. Mat. **2**, 9707–9711 (1990).

[23] E. Fawcett, Rev. Mod. Phys. **60** (1), 209–283 (1988).

[24] F. Chu, D. J. Thoma, Y. He, T. E. Mitchell, S. P. Chen, and J. H. Perepezki, Mat. Res. Soc. Symp. Proc. **364**, 1089–1094 (1995).

[25] A. Ormeci, F. Chu, J. M. Wills, T. E. Mitchell, R. C. Albers, D. J. Thoma, and S. P. Chen, Phys. Rev. B **54** (18), 12753–12762 (1996).

[26] O. Yifang, Z. Bangwei, L. Shuzhi, and J. Zhanpeng, Z. Phys. B **101**, 161–168 (1996).

[27] Z. Bangwei, O. Yifang, L. Shuzhi, and J. Zhanpeng, Physica B **262**, 218–225 (1999).

[28] J. Stadler, R. Mikulla, and H.-R. Trebin, Int. J. Mod. Phys. C **8** (5), 1131–1140 (1997).

[29] IMD, the ITAP Molecular Dynamics Program:
http://www.itap.physik.uni-stuttgart.de/~imd

[30] S. Hong and C. L. Fu, Intermetallics **7** (1), 5–9 (1999).

[31] B. Mayer, H. Anton, E. Bott, M. Methfessel, J. Sticht, J. Harris, and P. C. Schmidt, Intermetallics **11**, 23–32 (2003).

[32] D. J. Thoma and J. H. Perepezko, Mater. Sci. Eng. A **156**, 97–108 (1992).

[33] F. Chu, Y. He, D. J. Thoma, and T. E. Mitchell, Scripta Metall. et Mater. **33** (8), 1295–1300 (1995).

[34] F. F. Abraham, J. Mech. Phys. Solids **53** (5), 1071–1078 (2005).

[35] M. Dzugutov, Phys. Rev. A **46** (6), R2984–R2987 (1992).

[36] J. Roth, Phys. Rev. Lett. **79** (20), 4042 (1997).

[37] S. M. Foiles and J. B. Adams, Phys. Rev. B **40** (9), 5909–5915 (1989).

[38] J. R. Morris, C. Z. Wang, K. M. Ho, and C. T. Chan, Phys. Rev. B **49** (5), 3109–3115 (1994).

[39] Z. H. Jin, P. Gumbsch, K. Lu, and E. Ma, Phys. Rev. Lett. **87** (5), 055703 (2001).

[40] A. Al-Zu'bi et al., unpublished.

[41] A. A. Griffith, Philos. Trans. R. Soc. Lond. Ser. A **221**, 163–198 (1921).

[42] R. Thomson, C. Hsieh, and V. Rana, J. Appl. Phys. **42** (8), 3154–3160 (1971).

[43] C. T. Liu, J. H. Zhu, M. P. Brady, C. G. McKamey, and L. M. Pike, Intermetallics **8** (9-11), 1119–1129 (2000).

[44] T. Ohta, Y. Nakagawa, Y. Kaneno, H. Inoue, T. Takasugi, and W.-Y. Kim, J. Mater. Sci. **38** (4), 657–665 (2003).

[45] A. v. Keitz and G. Sauthoff, Intermetallics **10** (5), 497–510 (2002).